

**Resolving the Higgs-gluon coupling with jets**Malte Buschmann,<sup>1,2</sup> Christoph Englert,<sup>3</sup> Dorival Gonçalves,<sup>2</sup> Tilman Plehn,<sup>1</sup> and Michael Spannowsky<sup>2</sup><sup>1</sup>*Institut für Theoretische Physik, Universität Heidelberg, D-69120 Heidelberg, Germany*<sup>2</sup>*Institute for Particle Physics Phenomenology, Department of Physics, Durham University, Durham DH1 3LE, United Kingdom*<sup>3</sup>*SUPA, School of Physics and Astronomy, University of Glasgow, Glasgow G12 8QQ, United Kingdom*

(Received 3 June 2014; published 11 July 2014)

In the Standard Model, the Higgs coupling to gluons is almost entirely induced by top quark loops. We derive the logarithmic structure of Higgs production in association with two jets. Just like in the one-jet case, the transverse momentum distributions exhibit logarithms of the top quark mass and can be used to test the nature of the loop-induced Higgs coupling to gluons. Using Higgs decays to W bosons and to tau leptons, we show how the corresponding analyses hugely benefit from the second jet in the relevant signal rate as well as in the background rejection.

DOI: [10.1103/PhysRevD.90.013010](https://doi.org/10.1103/PhysRevD.90.013010)

PACS numbers: 14.80.Bn, 12.60.-i, 12.38.Aw

**I. INTRODUCTION**

After the recent discovery of a light, narrow, and likely fundamental Higgs boson [1,2], one of the main tasks of the upcoming LHC runs will be to study the properties of this new particle. An interesting aspect of the Higgs discovery is that it largely relies on higher-dimensional Higgs interactions which in the Standard Model (SM) are induced by loops of heavy quarks and gauge bosons. While this indirect information on Higgs coupling structures is complemented by precise tree-level information in the Higgs-gauge sector, our understanding of Higgs couplings to fermions largely relies on these loop effects.

This shortcoming is most obvious in our currently very limited and model-dependent understanding of the top Yukawa coupling [3–6]. A measurement of the top Yukawa coupling from associated Higgs and top production with a proper reconstruction of the heavy states will be challenging even in the upcoming LHC run [7–9]. This limitation is in stark contrast with our theoretical interest, where a measurement of the large top Yukawa coupling is crucial to extrapolate our understanding of the Higgs mechanism from LHC energy scales to more fundamental, high energies [10]. Beyond the Standard Model (BSM), this large size of the top Yukawa suggests that any new physics stabilizing the scalar Higgs mass should include a top partner, which in turn can contribute to the loop-induced Higgs couplings to gluons and photons [11].

To disentangle the Standard Model contribution, for example, to the Higgs-gluon coupling from new physics effects, we can use a particular feature of the Standard Model loops: in the presence of a Yukawa coupling, the associated dimension-6 operators no longer decouple. Instead, they induce a dimension-6 operator with a coupling strengths which approaches a finite value in the limit of large top masses. In this low energy limit, the interactions between any number of gluons and any number of

Higgs bosons is given by a simple effective Lagrangian [12,13]. While this approximation provides a very good prediction of the inclusive Higgs production rate, it leads to  $\mathcal{O}(10\%)$  deviations in most distributions for the  $gg \rightarrow H$  production process [14,15] and fails quite spectacularly for Higgs pair production [16]. Turning this argument around, we can use kinematic distributions in Higgs production processes to test our assumption that the Higgs-gluon interactions are induced by heavy quarks.

Physics beyond the Standard Model might also exhibit nondecoupling effects in the effective Higgs couplings. One such example is a fourth generation of chiral fermions, where the effects from new physics are of the same size as the Standard Model prediction. Because they are not described by a small parameter, such scenarios are largely ruled out altogether. In new physics extensions which do decouple, the characteristic small parameter is typically the ratio of the electroweak scale to the new physics mass scale. This mass ratio is constrained to be below  $\mathcal{O}(1/10)$ , with a possible exception of supersymmetric top partners which are experimentally still allowed to reside around the top mass scale [17]. Under this assumption of heavy new states, the low-energy approximation to the Higgs-gluon couplings holds for the loop contributions from physics beyond the Standard Model [18,19]. This makes it straightforward to interpret deviations from kinematic features predicted for the heavy quark loops in terms of new physics scenarios [20].

The key question in the above reasoning is which kinematic features are best suited to test the heavy quark origin of the Higgs-gluon couplings. It has been known for a long time that the transverse momentum distribution of Higgs production in association with a hard jet exhibits a logarithmic dependence on the top mass [18,19]. Recently, this effect has been proposed as a handle to test the Standard Model assumption that the Higgs-gluon coupling is exclusively due to heavy quark loops [21–25].

In this paper we for the first time study the structure of the top mass dependence in the production vertex beyond Higgs production with a single hard jet. Higgs production in gluon fusion associated with two hard initial-state radiation jets offers a much richer set of kinematic distributions.<sup>1</sup> It is well known that the correlations of the two initial-state radiation jets reflect the higher-dimensional structure of the Higgs coupling to gluons or any other hard process [26]. In this study we will use the two hard jets to extract the top mass dependence of the Higgs-gluon coupling.

First, we will show that the logarithmic top mass dependence in the vector boson fusion (VBF) topology is the same as for Higgs production with a single jet. Adding a second hard jet to the hard process [27] shifts a sizeable number of Higgs events from phase space regions which are not sensitive to top mass effects to regions which are sensitive. We will find that the sensitivity of the VBF topology to top mass effects should exceed the sensitivity

$$\mathcal{L}_{ggH} \supset g_{ggH} \frac{H}{v} G^{\mu\nu} G_{\mu\nu}$$

$$\frac{g_{ggH}}{v} = -i \frac{\alpha_s}{8\pi} \frac{1}{v} \tau [1 + (1 - \tau)f(\tau)] \quad f(\tau)^{\text{on-shell}} \stackrel{\tau \rightarrow \infty}{=} \left( \arcsin \sqrt{\frac{1}{\tau}} \right)^2 \tau \stackrel{\tau \rightarrow \infty}{=} \frac{1}{\tau} + \frac{1}{3\tau^2} + \mathcal{O}\left(\frac{1}{\tau^3}\right), \quad (1)$$

all in terms of  $\tau = 4m_t^2/m_H^2 > 1$ . Barring prefactors the function  $f$  corresponds to the scalar three-point function for a closed top loop. In the usual kinematic configuration for single Higgs production, the coupling  $g_{ggH}$  depends only on the top and Higgs masses, as indicated above. Once it appears as part of a more complex Feynman diagram, the coupling  $g_{ggH}$  will depend on the momenta of all three external states as well as on the top mass. This will become our main reason to define the hard process including two hard jets rather than one jet plus a parton shower.

In the simple low-energy limit, the interaction vertices between any number of gluons and any number of Higgs bosons can be described by the Lagrangian

$$\mathcal{L}_{ggH} = \frac{\alpha_s}{12\pi} \log\left(1 + \frac{H}{v}\right) G^{\mu\nu} G_{\mu\nu} \supset \frac{\alpha_s}{12\pi} \frac{H}{v} G^{\mu\nu} G_{\mu\nu}. \quad (2)$$

$$\begin{aligned} \mathcal{L}_{\text{int}} &\supset \left[ \kappa_t g_{ggH} + \kappa_g \frac{\alpha_s}{12\pi} \right] \frac{H}{v} G_{\mu\nu} G^{\mu\nu} - \kappa_t \frac{m_t}{v} H (\bar{t}_R t_L + \text{H.c.}) \quad \text{Refs. [24]} \\ &= (1 + \Delta_t + \Delta_g) g_{ggH} \frac{H}{v} G_{\mu\nu} G^{\mu\nu} - (1 + \Delta_t) \frac{m_t}{v} H (\bar{t}_R t_L + \text{H.c.}) \quad \text{SFITTER [3]}. \end{aligned} \quad (3)$$

<sup>1</sup>We will refer to this process as VBF and neglect the numerically small weak boson fusion contributions. Moreover, we do not require the usual forward tagging jets, but two hard jets defining the hard process together with the Higgs.

of the Higgs-plus-one-jet channel. Moreover, the VBF topology allows for a much improved background suppression in the  $H \rightarrow \tau\tau$  and  $H \rightarrow WW$  channels. This way, a second hard jet is not just an improvement of a dominant one-jet analysis; the two-jet hard process is more sensitive to top mass effects, the correlations of the second hard jet and the logarithmic top mass dependence are not covered by a parton shower description, and the second hard jet makes a big difference in the background rejection.

## II. TOP MASS EFFECTS

The main production process responsible for the Higgs discovery is gluon fusion, mediated by the Higgs coupling to a pair of gluons. This interaction does not exist at tree level, i.e., as part of the renormalizable dimension-4 Lagrangian. It is induced by heavy quarks, in the Standard Model dominantly via top quark loop [12,13],

The top Yukawa coupling in the top loop violates the decoupling theorem, so the interaction approaches a finite limit [12]. This nondecoupling property in combination with the absence of a dimension-4 Higgs coupling to gluons is unique to the dimension-6 operators mediating the Higgs couplings to gluons and photons, which are to a large degree responsible for the Higgs discovery [2].

One question which we have to answer based on LHC measurements is if the top Yukawa coupling is indeed responsible for the observed Higgs-gluon coupling or if other top partners contribute to the corresponding dimension-6 operator. In two different conventions, the relevant part of the Higgs interaction Lagrangian including a finite top mass and free couplings reads

We show the SFITTER conventions to indicate that the parameters  $\kappa_t$  and  $\kappa_g$  are indeed part of the usual LHC coupling analyses. The new aspect is to extract them from distributions rather than rates. As alluded to above, the dimension-6 operator is defined not only without any

reference to the top mass but also with the entire momentum dependence arising from the gluon field strengths. One physics scenario which could serve as an ultraviolet extension of Eq. (3) would be the Standard Model with an extended Higgs sector and an unobserved top partner [3,20]. Throughout this paper we will rely on two reference points unless otherwise mentioned,

$$(\kappa_t, \kappa_g)_{\text{SM}} = (1, 0) \quad \text{and} \quad (\kappa_t, \kappa_g)_{\text{BSM}} = (0.8, 0.2). \quad (4)$$

In the second point, the contributions from a top partner to a good approximation compensate for the reduced top Yukawa in the Higgs-gluon coupling, leaving the observed Higgs cross section at the LHC unchanged.

### A. Absorptive terms

Absorptive terms in the top loop inducing the effective Higgs-gluon coupling are well known from the behavior of the cross section as a function of the (formerly unknown) Higgs mass [13,15]. At  $m_H = 2m_t$  the formula for the scalar integral given in Eq. (1) develops an imaginary absorptive part, leading to a kink in the LHC cross section. Given the now fixed Higgs mass of 126 GeV, the question is how we can search for such effects at the LHC. For example, in Higgs production in association with two jets, the same absorptive parts should appear in the loop integrals shown in Fig. 1,

$$m_{Hj} = 2m_t \quad \text{and} \quad m_{Hjj} = 2m_t. \quad (5)$$

To illustrate the size of such absorptive effects, we study the process  $pp \rightarrow Hjj$  at the parton level in Fig. 2. It includes the loop-induced  $gggH$  interaction which indeed shows an absorptive part around  $m_{Hj} \sim 350$  GeV, as indicated in Eq. (5). We see that these absorptive parts are very small for both distributions and will hardly allow us to make a qualitative statement about the origin of the effective Higgs-gluon coupling, not even talking about a measurement of  $\kappa_t$  and  $\kappa_g$ .

### B. Top-induced logarithms

Higgs production in association with a hard jet probes a logarithmic top mass dependence of the loop-induced coupling [18,19]. This effect has recently been transformed

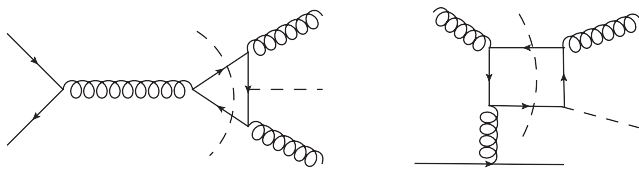


FIG. 1. Sample Feynman diagrams for the processes  $qq \rightarrow Hgg$  and  $gq \rightarrow Hgg$ , indicating the cuts which contribute to absorptive parts.

into a proposed experimental separation of the coupling modifications  $\kappa_t$  and  $\kappa_g$  in this production channel [20,21,23,24]. In the high-energy limit, or for small top and Higgs masses, the leading term of the matrix element for the partonic subprocess  $gg \rightarrow Hg$  scales like

$$|\mathcal{M}_{Hj}|^2 \propto m_t^4 \log^4 \frac{p_T^2}{m_t^2}. \quad (6)$$

The transverse momentum constitutes the external energy scale in the limit of  $p_T \gg m_H, m_t$ . If the effective Higgs-gluon coupling is not induced by the top quark, this logarithm does not occur.

Next, we look at the logarithmic structure for the more complex final state of Higgs production in association with two jets. In the presence of several external mass scales, it is not clear which final-state invariant drives the logarithmic top mass dependence. The simplest subprocess  $q\bar{q} \rightarrow q\bar{q}H$  only probes the effective  $ggH$  coupling, but with two off-shell gluons at sizeable virtualities. In terms of the virtualities of  $Q_{1,2} > 0$  of the spacelike or  $t$ -channel gluons, the corresponding scalar three-point function scales like

$$|\mathcal{M}_{Hjj}|^2 \propto \frac{m_t^4}{(Q_1^2 - Q_2^2)^2} \left( \log^2 \frac{Q_1^2}{m_t^2} - \log^2 \frac{Q_2^2}{m_t^2} \right)^2 \stackrel{Q_1 \gg Q_2}{\approx} \frac{m_t^4}{Q_1^4} \times \log^4 \frac{Q_1^2}{m_t^2}. \quad (7)$$

In the collinear limit, the virtuality of the incoming parton splitting is linked to the transverse momentum of the forward tagging jet through a simple linear transformation. Logarithms in the virtuality can be directly translated into logarithms of the transverse momentum, independent if they are scaling logarithms which get absorbed into the parton densities or if they affect the hard process [28].

In the limit of one significantly harder tagging jet  $Q_1 \gg Q_2$  recoiling against the Higgs boson, the diagrams in the vector boson fusion topology scale like

$$|\mathcal{M}_{Hjj}|^2 \propto m_t^4 \log^4 \frac{p_{T,j}^2}{m_t^2} \sim m_t^4 \log^4 \frac{p_{T,H}^2}{m_t^2}. \quad (8)$$

In this step we assume a linear relation between the virtuality and the transverse momentum of the additional jets [28]. In the left panel of Fig. 3, we show the correlation between the leading  $p_{T,j}$  and the corresponding gluon virtuality for the SM hypothesis and clearly see the expected correlation with  $p_{T,j} > Q$ . Away from the diagonal, we only find events with  $p_{T,j_1} < Q_1$ , in agreement with the kinematic considerations of Ref. [28]. This pattern gets transferred to the transverse momentum of the recoiling Higgs. In the right two panels, we show the same kinematic correlation for the ratio SM/BSM. We see the same increase

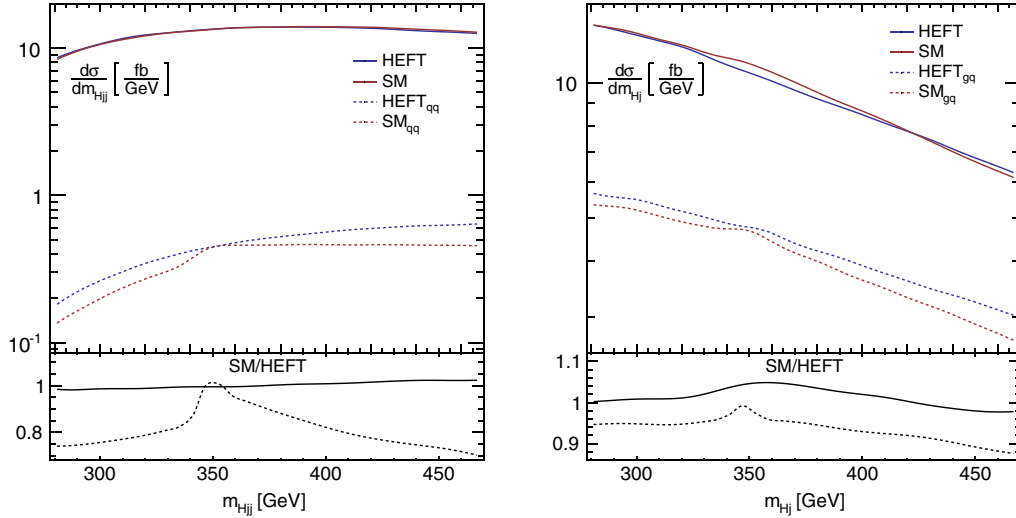


FIG. 2 (color online). Differential distributions for  $m_{Hjj}$  (left) and for  $m_{Hj}$  (right) for the  $Hjj$  process. The Standard Model curves include the full top mass dependence, while the low-energy effective field theory approximation (HEFT) relies on the approximation in Eq. (2). The index  $qq$  ( $gg$ ) indicates Feynman diagrams with an incoming quark pair (gluon quark). We assume  $\sqrt{S} = 13$  TeV.

of the dimension-6 operators at larger transverse momenta as in the  $Hj$  channel [20,21,23,24]. For given  $p_{T,j_1}$  values, this ratio is independent of the virtuality. This means that while the virtuality is fixed by the steep gluonic parton densities the top mass logarithm feeds on the transverse momentum and the jet momentum in the beam direction.

After ensuring that the top mass logarithms in  $Hj$  and  $Hjj$  have the same origin, we can compare their numerical impact. In Fig. 4 we show the dependence of the  $Hj$  and  $Hjj$  production rates on the transverse momentum of the leading tagging jet and the Higgs, based on the MCFM [29] and VBFNLO [30] implementations. We have validated this modified MCFM dimension-6 setup against an independent implementation based on VBFNLO. We compare the prediction of the Standard Model  $\kappa_{t,g} = (1, 0)$  to an additional BSM contribution from the dimension-6 operator  $\kappa_{t,g} = (0.8, 0.2)$ , as defined in Eq. (4). For both channels there appears a logarithmic enhancement for transverse momenta larger than twice the top mass.

The full  $Hjj$  production process includes one-loop triangle, box, and pentagon contributions, which cannot be separated. However, the different  $qq$ ,  $gq$ , and  $gg$  initial states offer a handle to determine the size of their relative contributions. For the  $qq$  and  $gq$  initial states, we have triangle and box diagrams, and the  $gg$  initial state will include pentagons. For all initial states, we find an enhanced dimension-6 BSM component at large Higgs and jet transverse momenta. The effect is strongest for incoming quarks and less pronounced for pure gluon amplitudes. This confirms our original assumption that the top mass logarithm arises from the VBF topology with an effective triangular  $ggH$  interaction for all initial states. This topology is approximately added to the  $Hj$  simulation once we include a parton shower to simulate initial-state radiation. However, if both jets are hard, the VBF topology is correctly described by the appropriate hard process, which includes the Higgs as well as two jets.

The comparison of the  $Hj$  and the  $Hjj$  channels in Fig. 4 also shows that for one recoiling jet most of the cross

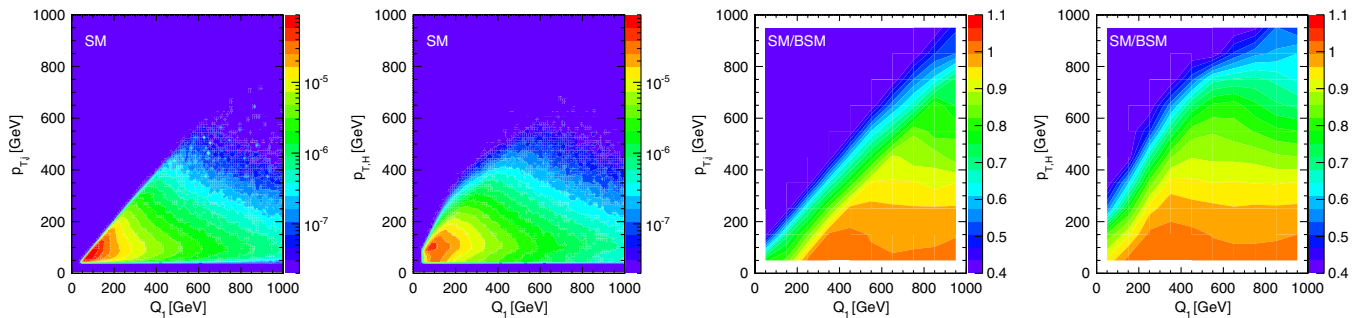


FIG. 3 (color online). Left to right: correlation plots for the leading  $p_{T,j}$  vs  $Q_1$  and  $p_{T,H}$  vs  $Q_1$  for  $Hjj$  production in the Standard Model,  $\kappa_{t,g} = (1, 0)$ . We also show the ratio SM/BSM, where BSM is defined as  $\kappa_{t,g} = (0.8, 0.2)$ .



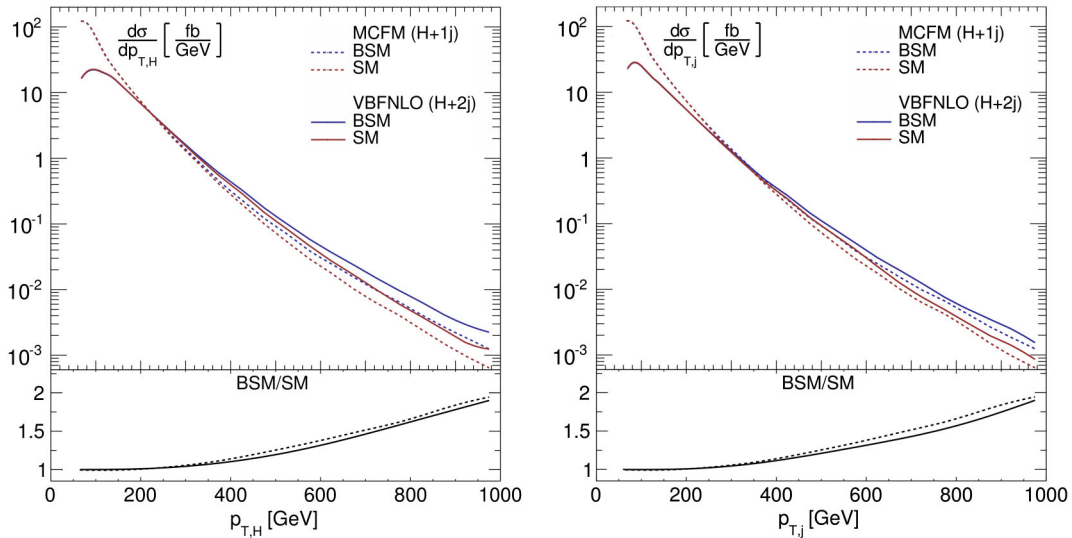


FIG. 4 (color online). Parton-level  $p_{T,H}$  (left) and  $p_{T,j_1}$  (right) distributions for  $Hj$  and  $Hjj$  production. The red curve corresponds to the Standard Model  $\kappa_{t,g} = (1, 0)$ , while the blue curves follow from the BSM hypothesis  $\kappa_{t,g} = (0.8, 0.2)$ . We assume  $\sqrt{S} = 13$  TeV.

section comes from phase space regions which do not resolve the effective Higgs-gluon coupling. In comparison, for two hard jets recoiling against the boosted Higgs, the drop in the total cross section appears exclusively in the insensitive regime, while even in terms of absolute event numbers the sensitivity to the top mass logarithm increases. If indeed the hard  $Hjj$  process is numerically more relevant in the high- $p_T$  regime than the hard  $Hj$  process, we need to worry about even more jets. We can only speculate about this, but from the above observation that the top mass logarithm arises from the VBF topology, the third jet would be most helpful if arising from a final-state splitting. Such configurations should be reasonably well described by the final-state parton shower.

After isolating the top mass logarithm in the transverse momentum spectra for  $Hjj$  production given by Eq. (8), we need to sadly convince ourselves that there are no

additional top mass logarithms in this process. For example, there could be very promising logarithms in the largest momentum scale, i.e.,  $\log m_{jj}/m_t$ . In Fig. 5 we show the  $m_{jj}$  distribution as well as the leading  $p_{z,j_1}$  and  $p_{z,H}$  distributions for  $Hjj$  production. For the top-induced coupling and the dimension-6 coupling, they are perfectly aligned, indicating that none of these observables is affected by top mass logarithms. The top mass dependence really only appears in the transverse momentum spectra. In the following we will focus on the transverse momentum of the Higgs, while eventually an experimental analysis could include both  $p_{T,H}$  and the leading  $p_{T,j}$ .

### C. Including the interference

Based on the interaction Lagrangian in Eq. (3), we can easily translate the modified coupling strengths into

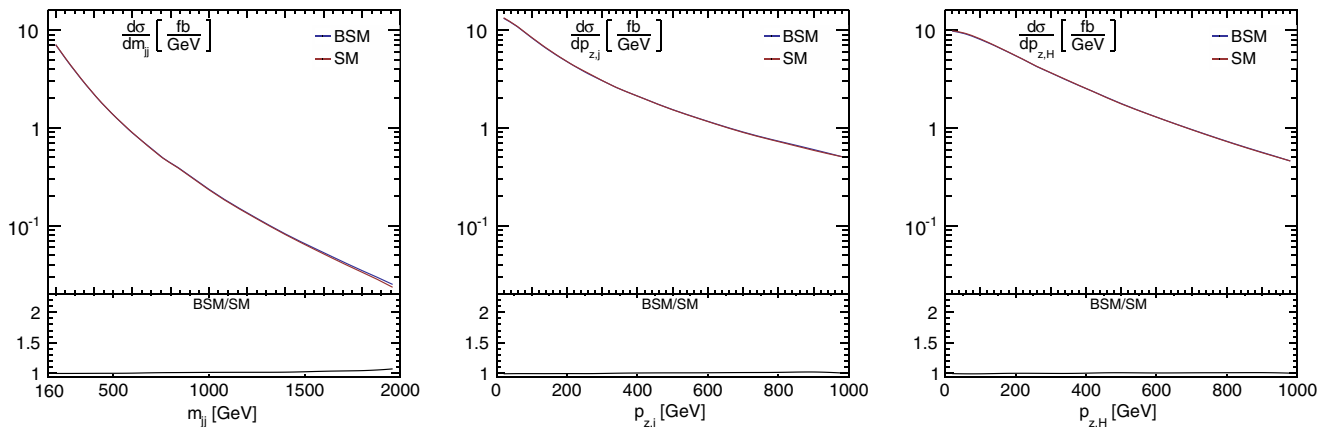


FIG. 5 (color online). Parton-level  $m_{jj}$  (left),  $p_{z,j_1}$  (center), and  $p_{z,H}$  (right) distributions for  $Hjj$  production.

differential or total LHC cross sections. For simplicity, we keep all other tree-level Higgs interactions unchanged, so the expected slight shift in the photon-Higgs coupling will be of no phenomenological relevance. The matrix element for Higgs production in gluon fusion is based on the  $HG_{\mu\nu}G^{\mu\nu}$  interaction and will consist of two terms,

$$\mathcal{M} = \kappa_t \mathcal{M}_t + \kappa_g \mathcal{M}_g, \quad (9)$$

where the index  $g$  indicates the dimension-6 operator contribution and all prefactors except for the  $\kappa_j$  are absorbed in the definitions of  $\mathcal{M}_j$ . For the matrix element squared and any kinematic distributions, this means

$$\frac{d\sigma}{d\mathcal{O}} = \kappa_t^2 \frac{d\sigma_{tt}}{d\mathcal{O}} + \kappa_t \kappa_g \frac{d\sigma_{tg}}{d\mathcal{O}} + \kappa_g^2 \frac{d\sigma_{gg}}{d\mathcal{O}}, \quad (10)$$

where for small deviations from the Standard Model the last term will be numerically irrelevant. In Fig. 6 we present the three transverse momentum distributions for the Higgs, on which we will rely for the remaining analysis. To be consistent, we use MCFM + PYTHIA8 [29,31] for the hard  $Hj$  production process with the scale choice  $\mu_F^2 = \mu_R^2 = m_H^2 + p_{T,j}^2$  and VBFNLO + PYTHIA8 [30,31] for the hard  $Hjj$  production process with the scale choice  $\mu_F^2 = \mu_R^2 = m_H^2 + p_{T,j1}^2 + p_{T,j2}^2$ . For example, the slight broadening of the low- $p_T$  peaks compared to Fig. 4 is due to parton shower effects and this scale choice. The full simulation confirms that the  $Hj$  process has a larger total rate than the  $Hjj$  process, but this additional  $Hj$  rate is concentrated at small transverse momenta and does not carry information on the Higgs-gluon coupling. For  $p_{T,H} > 300$  GeV the

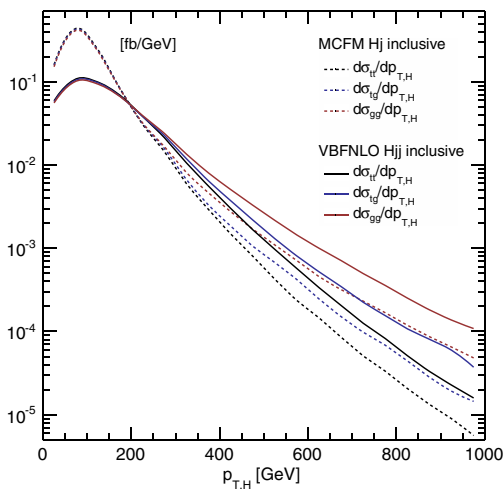


FIG. 6 (color online). Transverse momentum distribution for  $Hj$  production (based on MCFM) and  $Hjj$  production (based on VBFNLO). Both codes use PYTHIA8 for the parton shower. The top-induced and dimension-6 contributions as well as their interference are defined in Eq. (10). We assume  $\sqrt{S} = 13$  TeV and for technical reasons include a decay  $H \rightarrow \tau\tau$  with minimal cuts.

parton shower is expected to underestimate additional jet radiation off the  $Hj$  process and cannot be expected to reflect the top mass logarithms; hence, the  $Hjj$  process gives a larger relevant number of events to probe the Higgs-gluon vertex. This is universally true for all three contributions defined in Eq. (10).

### III. SIGNAL-BACKGROUND ANALYSES

Following the results in the last section, the key question becomes how much, in addition to the increase in the number of relevant signal events, the background rejection benefits from the additional jet in the hard process. As simple examples we consider the two most promising Higgs decay channels,  $H \rightarrow WW$  and  $H \rightarrow \tau\tau$ , in the fully leptonic decay modes at the LHC with  $\sqrt{S} = 13$  TeV. Besides the dominant Higgs production in gluon fusion, there are of course other Higgs productions which can contribute to our signature. To allow for a clean interpretation of the results, we ensure that Higgs-strahlung with heavy quarks in the final state is negligible, in particular because of our  $b$  veto meant to reduce the top pair background.

The signal events are generated with MCFM [29] for the  $Hj$  process and with VBFNLO [30] for the  $Hjj$  process, respectively. They are showered with PYTHIA8 [31]. Both generators provide results for finite top mass,  $\kappa_{t,g} = (1, 0)$ , as well as the pure dimension-6 scenario  $\kappa_{t,g} = (0, 1)$ . To probe the whole  $\kappa_t$  vs  $\kappa_g$  range, we expand both implementations including the complete interference structure given in Eq. (10). Because there are no next-to-leading order (NLO) computations available for either of the two channels with full top mass dependence, we scale our total cross sections to the corresponding NLO rates in the heavy top limit. For a consistent scale choice, we apply a flat correction of  $K_{Hj} \sim 1.4$  [29] and  $K_{Hjj} \sim 1.6$  [32]. In particular for the two-jet case, it is known that distributions are reproduced at the 10% level even for highly boosted Higgs bosons when the full top mass dependence is included at leading order [14].

The  $t\bar{t}$  + jets and  $WW$  + jets background are generated with the POWHEGBOX [33], showered with a vetoed PYTHIA8 shower [31]. We also include the  $Z$  + jets background from SHERPA + BLACKHAT [34] merged at next-to-leading order with up to three hard jets. In all background processes, we enforce top,  $W$ , and  $Z$  decays to charged leptons, i.e., muons, electrons, or taus. Jets are defined using the anti- $k_T$  algorithm implemented in FASTJET [35] with  $R = 0.5$  and

$$p_{T,j} > 40 \text{ GeV}, \quad \text{and} \quad |y_j| < 4.5. \quad (11)$$

If explicitly shown, the one or two recoil jets are defined as the hardest jets fulfilling this requirement. Throughout we smear the missing energy vector using a Gaussian. For the leptons we require two isolated opposite-sign leptons with

TABLE I. Cut flow for  $H + \text{jets}$ ,  $WW + \text{jets}$ , and  $t\bar{t} + \text{jets}$ . All rates are given in fb.

Cuts	$Hj \rightarrow (WW)j$ inclusive			$Hjj \rightarrow (WW)jj$ inclusive		
	$H + \text{jets}$	$WW + \text{jets}$	$t\bar{t} + \text{jets}$	$H + \text{jets}$	$WW + \text{jets}$	$t\bar{t} + \text{jets}$
$p_{T,j} > 40 \text{ GeV},  y_j  < 4.5$	35.5	524	14770	17.3	90.7	7633
$p_{T,\ell} > 20 \text{ GeV},  y_\ell  < 2.5$						
$N_b = 0$	33.3	515	4920	15.2	87.4	1690
$m_{\ell\ell} \in [10, 60] \text{ GeV}$	28.3	106	1060	13.0	17.2	351
$E_T > 45 \text{ GeV}$	21.4	92.9	930	10.6	15.9	309
$\Delta\phi_{\ell\ell} < 0.8$	14.3	49.8	479	8.14	10.3	162
$m_T < 125 \text{ GeV}$	14.2	26.6	220	8.09	6.14	76.2
$p_{T,H} > 300 \text{ GeV}$	0.59	2.73	5.18	1.06	1.39	3.28
$\Delta\phi_{jj} < 1.8$				0.87	1.05	1.33
$p_{T,j1}/p_{T,j2} < 2.5$				0.57	0.53	0.53

$$p_{T,\ell} > 20 \text{ GeV}, \quad \text{and} \quad |y_\ell| < 2.5, \quad (12)$$

where the isolation criterion is a hadronic energy deposition  $E_{T,\text{had}} < E_{T,\ell}/10$  within a cone of size  $R = 0.2$ . To suppress the top background, we require zero  $b$  tags with a flat tagging efficiency of 70% and a mistag rate of 2%. Our simulation of the top pair background should be taken with a grain of salt because there are many ways of further suppressing this background based on the underlying jet structure [36]. Note that the focus of this signal and background analysis is not to estimate a realistic target for the measurement of  $\kappa_t$  and  $\kappa_g$ , but to see how the  $Hjj$  process compares with the  $Hj$  process [20,21,23,24].

### A. $H \rightarrow WW$ decays

As the first signature, we show how we can probe the structure of the Higgs-gluon coupling in  $Hjj$  production based on leptonic  $H \rightarrow WW$  decays. To estimate the additional benefit of including the second jet, we compare the signal-to-background ratios  $S/B$  for Higgs production with one and two hard jets. For the  $WW$  decay channel, the main backgrounds are  $WW + \text{jets}$  and  $t\bar{t} + \text{jets}$  production. We start with the basic cuts shown in the first lines of Tab. I.

Aside from the missing weak boson fusion characteristics, they are similar to the known analysis techniques for Higgs production in association with two jets. Obviously, we do not apply a stiff  $m_{jj}$  cut to reduce QCD backgrounds as well as gluon fusion Higgs production. The transverse mass of the  $WW$  system is defined as

$$m_T^2 = (E_T^{\ell\ell} + E_T)^2 - |\vec{p}_T^{\ell\ell} + \vec{E}_T|^2 \quad \text{with} \\ E_T^{\ell\ell} = \sqrt{|\vec{p}_T^{\ell\ell}|^2 + m_{\ell\ell}^2}. \quad (13)$$

The  $p_{T,H}$  cut extracts events which are sensitive to the logarithmic dependence on the top mass. The numbers shown for the  $Hj$  process are in good agreement with the findings of Ref. [20]. As expected from Fig. 6, the number of signal events in the  $Hjj$  process exceeds the corresponding number in the  $Hj$  channel by a factor of 2. Moreover, in particular the  $WW + \text{jets}$  background is reduced by the required second hard jet.

In addition, we can use the second jet to define additional observables which can in turn be used to suppress backgrounds. Two choices, namely, the azimuthal angle between the tagging jets [26] and the ratio of transverse

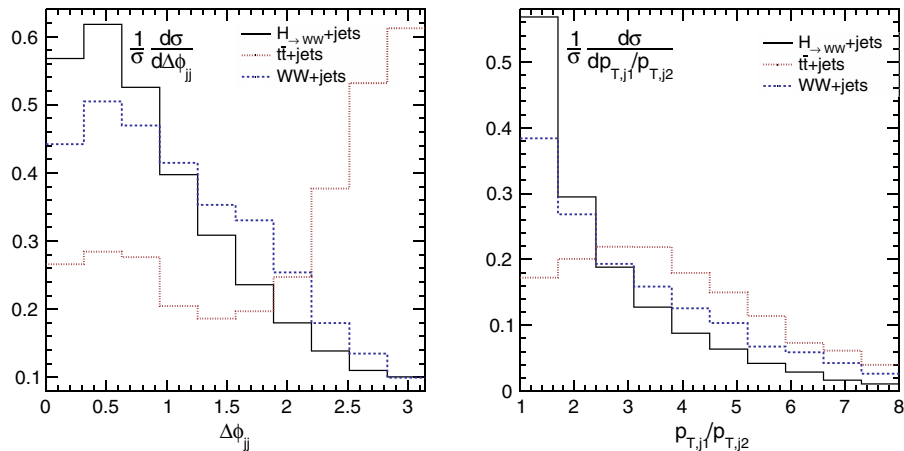


FIG. 7 (color online). Normalized  $\Delta\phi_{jj}$  (left) and  $p_{T,j1}/p_{T,j2}$  (right) distributions for the  $H \rightarrow WW$  signal and the dominant backgrounds. All universal cuts listed in Table I are already applied.

TABLE II. Cut flow for  $H$ +jets,  $Z/\gamma^*$  + jets,  $WW$  + jets, and  $t\bar{t}$  + jets. All rates are given in fb.

Cuts	$Hj \rightarrow (\tau\tau)j$ inclusive				$Hjj \rightarrow (\tau\tau)jj$ inclusive			
	$H$ + jets	$Z/\gamma^*$ + jets	$WW$ + jets	$t\bar{t}$ + jets	$H$ + jets	$Z/\gamma^*$ + jets	$WW$ + jets	$t\bar{t}$ + jets
$p_{T,j} > 40$ GeV, $ y_j  < 4.5$	9.82	162303	524	14770	5.10	27670	90.7	7633
$p_{T,\ell} > 20$ GeV, $ y_\ell  < 2.5$								
$N_b = 0$	9.21	148221	515	4920	4.50	23218	87.4	1690
$m_{\ell\ell} \in [10, 60]$ GeV	6.59	10466	179	1616	3.41	1832	28.3	541
$m_{\ell\ell'} \in [10, 100]$ GeV								
$E_T > 45$ GeV	6.24	38.1	166	1616	3.31	0.65	27.0	541
$ m_{\tau\tau} - m_H  < 20$ GeV	5.88	2.84	6.28	45.9	3.10	0.11	1.18	16.0
$p_{T,H} > 300$ GeV	0.23	0.013	0.40	0.87	0.41	0.004	0.20	0.56
$\Delta\phi_{jj} < 1.8$					0.33	0	0.15	0.22
$p_{T,j1}/p_{T,j2} < 2.5$					0.22	0	0.076	0.086

momenta of the two jets, are shown in Fig. 7. It is interesting to notice that the usual application of the azimuthal angle between the tagging jets relies on the forward jet kinematics, while in this analysis the tagging jets are hard and relatively central. First, we see that the boosted Higgs configuration forces the two recoil jets for the Higgs signal and the  $WW$  background to move close to each other in the azimuthal plane. In addition, two jets recoiling against one Higgs boson prefers more balanced jet momenta than the recoil against two independently produced  $W$  bosons. This again supports our earlier conclusion that the underlying hard process indeed includes two hard jets. Cutting on both jet-jet correlations, we can reduce the  $WW$  background to the  $Hjj$  signal to roughly a fifth of the corresponding  $Hj$  background, for similar signal rates in the boosted phase space region.

### B. $H \rightarrow \tau\tau$ decays

As an alternative decay signature, we also study  $Hjj$  production with a purely leptonic  $H \rightarrow \tau\tau$  decay. Because the leptonic  $WW$  and  $\tau\tau$  decay channels have a similar detector signature and main backgrounds are  $t\bar{t}$  + jets and  $WW$  + jets, we stick to a similar initial analysis strategy,

now shown in Table II. Instead of the transverse mass cut, we compute  $m_{\tau\tau}$  in the collinear approximation [18],

$$m_{\tau\tau} = \frac{m_{\text{vis}}}{\sqrt{x_1 x_2}} \quad \text{with} \quad x_{1,2} = \frac{p_{\text{vis}1,2}}{p_{\text{vis}1,2} + p_{\text{miss}1,2}}, \quad (14)$$

where  $m_{\text{vis}}$  and  $p_{\text{vis}}$  are the invariant mass and total momentum of the visible tau decay products. The variable  $p_{\text{miss}}$  is the neutrino momentum reconstructed in the collinear approximation. Using this approximation we require

$$|m_{\tau\tau} - m_H| < 20 \text{ GeV}, \quad \text{with} \quad x_{1,2} \in [0.1, 1]. \quad (15)$$

This large mass window should include the vast majority of signal events, while we will see that it is still sufficient to control the backgrounds. By imposing

$$p_{T,H} \sim p_{T,\ell_1} + p_{T,\ell_2} + p_T > 300 \text{ GeV}, \quad (16)$$

we ensure perfect kinematical conditions to apply the collinear approximation. Similar to the  $WW$  channel, we then use the second jet to further suppress the backgrounds; see Fig. 8. As for the  $WW$  case, we see that for similar event

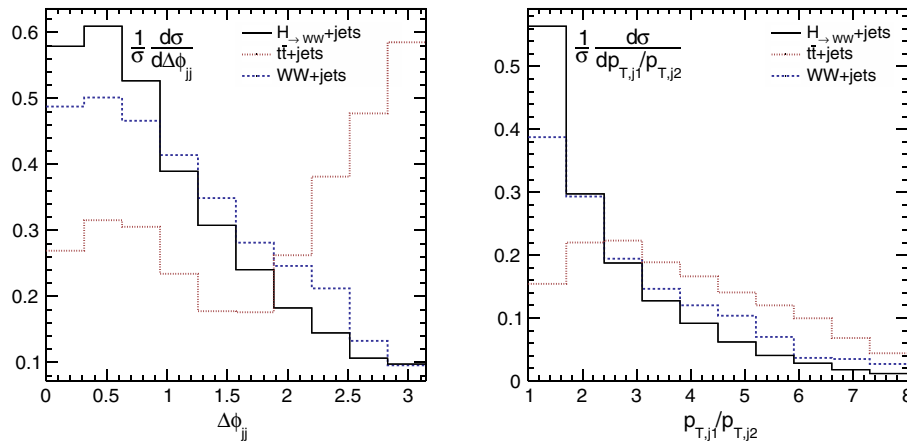


FIG. 8 (color online). Normalized  $\Delta\phi_{jj}$  (left) and  $p_{T,j1}/p_{T,j2}$  (right) distributions for the  $H \rightarrow \tau\tau$  signal and the dominant backgrounds. All universal cuts listed in Table II are already applied.



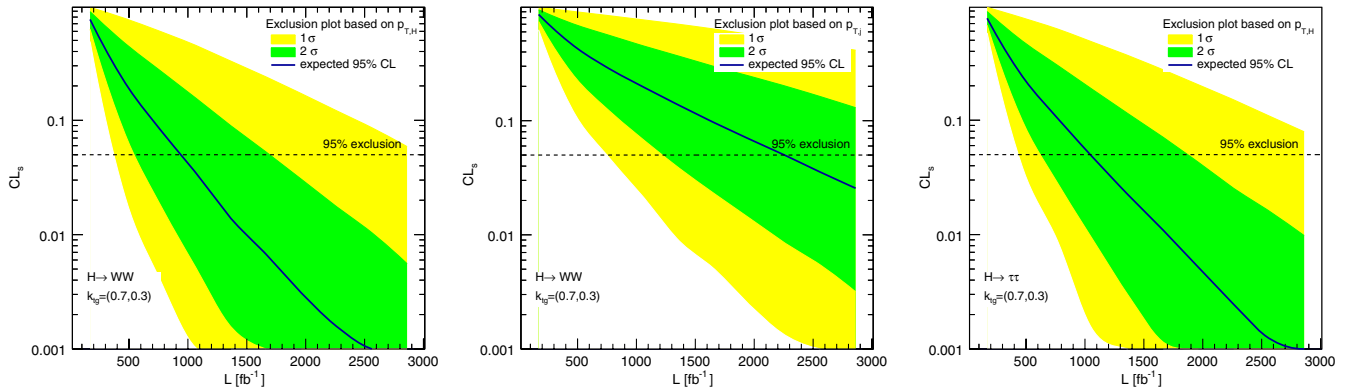


FIG. 9 (color online). Confidence level for separating the BSM hypotheses  $\kappa_{t,g} = (0.7, 0.3)$  from the Standard Model. We show results for  $H \rightarrow WW$  decays based on the transverse momentum of the Higgs (left) and the hardest jet (center). For the  $H \rightarrow \tau\tau$  decays (right), we limit ourselves to the more promising case of the Higgs transverse momentum.

numbers in the top-mass-sensitive region the backgrounds in the  $Hjj$  analysis are something like a factor 1/5 smaller than for the  $Hj$  case.

Combining the different  $p_{T,H}$  bins into a shape analysis allows us to extract information on the parameters  $\kappa_t$  and  $\kappa_g$  introduced in Eq. (3). To estimate the power of the  $Hjj$  analysis, we evaluate the  $p_{T,H}$  distribution using the  $CL_s$  method. The Standard Model  $\kappa_{t,g} = (1, 0)$  defines the null hypothesis, to be compared with the BSM parameter point  $\kappa_{t,g} = (0.7, 0.3)$ . For the results shown in Fig. 9, we assume a NLO scale uncertainty of  $\mathcal{O}(20\%)$  [30]. We also show results for the leading  $p_{T,j}$  distribution, indicating that the Higgs transverse momentum is the best-suited single observable for the  $Hjj$  analysis. Unlike for the  $Hj$  analysis, we find that the leptonic  $WW$  and  $\tau\tau$  decays are similarly promising.

As indicated by Fig. 9, excluding small deviations of the Higgs top and Higgs gluon from their Standard Model values couplings remains a challenge for the upcoming LHC runs. To accumulate the best sensitivity possible, it will be necessary to combine all available channels. However, cleanly separating the leptonic  $H \rightarrow \tau\tau$  and  $H \rightarrow WW$  decays in  $Hj$  production is kinematically very difficult [20]. In this study we now find that  $Hjj$  production with a decay  $H \rightarrow WW$  is almost as sensitive as the corresponding  $\tau\tau$  decay channel, so with full control over the additional one or two jets, a combination of the two decay channels seems possible.

#### IV. CONCLUSIONS

We have shown that the extraction of the top mass dependence in the effective Higgs-gluon coupling at the LHC benefits from a second jet, a hard process consisting of the Higgs plus two jets. As two robust example signatures, we consider purely leptonic Higgs decays to  $W$  bosons and  $\tau$  leptons. Higgs production with two hard

jets should not be considered a correction to Higgs production plus one jet in the boosted regime, because in the corresponding analysis we find:

- (1) the divergence structure of the  $Hjj$  process is given by a similar logarithm as the  $Hj$  case; numerically, the VBF topology with two hard jets radiated off the initial state partons dominates the top mass dependence at large transverse momenta.
- (2) adding a second hard jet moves a large fraction of signal events from top-mass-insensitive phase space regions to top-mass-sensitive configurations. For large transverse momenta of the Higgs boson, the  $Hjj$  production process even contributes more signal events than the  $Hj$  process.
- (3) a second fully correlated jet described by the hard matrix element can be used to reduce the backgrounds by roughly a factor 1/5 for a similar number of signal events, compared to the same analysis with only one hard jet.
- (4) both the  $H \rightarrow WW$  and  $H \rightarrow \tau\tau$  signatures appear feasible when combined with the  $Hjj$  production process.

Given the statistical limitation of this detailed study of the Higgs-gluon coupling and its underlying loop structure, the  $Hjj$  channel should be a very useful additional handle. Obviously, a fully merged analysis of the  $Hj$  and  $Hjj$  channels including the complete Higgs-gluon coupling structure will combine the two available channels, for example, in the  $p_{T,H}$  distribution.

#### ACKNOWLEDGMENTS

We would like to thank Marek Schönherr for his kind help with all kinds of QCD issues and Michael Spira for valuable discussions. C. E. is supported by the Institute for Particle Physics Phenomenology Associateship program.

- [1] P. W. Higgs, *Phys. Lett.* **12**, 132 (1964); P. W. Higgs, *Phys. Rev. Lett.* **13**, 508 (1964); P. W. Higgs, *Phys. Rev.* **145**, 1156 (1966); F. Englert and R. Brout, *Phys. Rev. Lett.* **13**, 321 (1964); G. S. Guralnik, C. R. Hagen, and T. W. Kibble, *Phys. Rev. Lett.* **13**, 585 (1964).
- [2] G. Aad *et al.* (ATLAS Collaboration), *Phys. Lett. B* **716**, 1 (2012); S. Chatrchyan *et al.* (CMS Collaboration), *Phys. Lett. B* **716**, 30 (2012).
- [3] M. Klute, R. Lafaye, T. Plehn, M. Rauch, and D. Zerwas, *Phys. Rev. Lett.* **109**, 101801 (2012); D. Lopez-Val, T. Plehn, and M. Rauch, *J. High Energy Phys.* **10** (2013) 134.
- [4] ATLAS Collaboration, ATLAS-CONF-2012-170; CMS Collaboration, CMS-PAS-HIG-12-045.
- [5] A. Azatov, R. Contino, and J. Galloway, *J. High Energy Phys.* **04** (2012) 127; P. P. Giardino, K. Kannike, M. Raidal, and A. Strumia, *Phys. Lett. B* **718**, 469 (2012); J. Ellis and T. You, *J. High Energy Phys.* **09** (2012) 123; J. R. Espinosa, C. Grojean, M. Mühlleitner, and M. Trott, *J. High Energy Phys.* **05** (2012) 097; **09** (2012) 126; **12** (2012) 045; A. Djouadi and G. Moreau, *Eur. Phys. J. C* **73**, 2512 (2013); J. Ellis and T. You, *J. High Energy Phys.* **06** (2013) 103.
- [6] For recent discussions of dimension-6 operators, see, e.g., A. Azatov and J. Galloway, *Int. J. Mod. Phys. A* **28**, 1330004 (2013); I. Brivio, T. Corbett, O. J. P. Éboli, M. B. Gavela, J. Gonzalez-Fraile, M. C. Gonzalez-Garcia, L. Merlo, and S. Rigolin, *J. High Energy Phys.* **03** (2014) 024; R. Contino, M. Ghezzi, C. Grojean, M. Mühlleitner, and M. Spira, *J. High Energy Phys.* **07** (2013) 035; J. Elias-Miro, J. R. Espinosa, E. Masso, and A. Pomarol, *J. High Energy Phys.* **11** (2013) 066; C. Englert, A. Freitas, M. Mühlleitner, T. Plehn, M. Rauch, M. Spira, and K. Walz, [arXiv:1403.7191](https://arxiv.org/abs/1403.7191); J. Ellis, V. Sanz and T. You, [arXiv:1404.3667](https://arxiv.org/abs/1404.3667).
- [7] A. Belyaev and L. Reina, *J. High Energy Phys.* **08** (2002) 041; E. Gross and L. Zivkovic, *Eur. Phys. J. C* **59**, 731 (2009); T. Plehn, G. P. Salam, and M. Spannowsky, *Phys. Rev. Lett.* **104**, 111801 (2010); C. Boddy, S. Farrington, and C. Hays, *Phys. Rev. D* **86**, 073009 (2012); P. Artoisenet, P. de Aquino, F. Maltoni, and O. Mattelaer, *Phys. Rev. Lett.* **111**, 091802 (2013); P. Agrawal, S. Bandyopadhyay, and S. P. Das, [arXiv:1308.6511](https://arxiv.org/abs/1308.6511); M. R. Buckley, T. Plehn, T. Schell, and M. Takeuchi, *J. High Energy Phys.* **02** (2014) 130.
- [8] M. Farina, C. Grojean, F. Maltoni, E. Salvioni, and A. Thamm, *J. High Energy Phys.* **05** (2013) 022; S. Biswas, E. Gabrielli, F. Margaroli, and B. Mele, *J. High Energy Phys.* **07** (2013) 073; J. Ellis, D. S. Hwang, K. Sakurai, and M. Takeuchi, *J. High Energy Phys.* **04** (2014) 004; C. Englert and E. Re, *Phys. Rev. D* **89**, 073020 (2014).
- [9] W. J. Stirling and D. J. Summers, *Phys. Lett. B* **283**, 411 (1992); F. Maltoni, D. L. Rainwater, and S. Willenbrock, *Phys. Rev. D* **66**, 034022 (2002).
- [10] See, e.g., M. Shaposhnikov and C. Wetterich, *Phys. Lett. B* **683**, 196 (2010); M. Holthausen, K. S. Lim, and M. Lindner, *J. High Energy Phys.* **02** (2012) 037; A. Hebecker, A. K. Knochel, and T. Weigand, *Nucl. Phys.* **B874**, 1 (2013); D. Buttazzo, G. Degrandi, P. Paolo Giardino, G. F. Giudice, F. Sala, A. Salvio, and A. Strumia, *J. High Energy Phys.* **12** (2013) 089.
- [11] D. E. Morrissey, T. Plehn, and T. M. P. Tait, *Phys. Rep.* **515**, 1 (2012).
- [12] J. R. Ellis, M. K. Gaillard, and D. V. Nanopoulos, *Nucl. Phys.* **B106**, 292 (1976); M. A. Shifman, A. I. Vainshtein, M. B. Voloshin, and V. I. Zakharov, *Yad. Fiz.* **30**, 1368 (1979) [*Sov. J. Nucl. Phys.* **30**, 711 (1979)]; B. A. Kniehl and M. Spira, *Z. Phys. C* **69**, 77 (1995).
- [13] For a pedagogical introduction, see, e.g., T. Plehn, *Lect. Notes Phys.* **844**, 1 (2012).
- [14] D. Graudenz, M. Spira, and P. M. Zerwas, *Phys. Rev. Lett.* **70**, 1372 (1993); M. Spira, A. Djouadi, D. Graudenz, and P. M. Zerwas, *Nucl. Phys.* **B453**, 17 (1995); M. Krämer, E. Laenen, and M. Spira, *Nucl. Phys.* **B511**, 523 (1998); S. Marzani, R. D. Ball, V. Del Duca, S. Forte, and A. Vicini, *Nucl. Phys.* **B800**, 127 (2008); A. Pak, M. Rogal, and M. Steinhauser, *J. High Energy Phys.* **02** (2010) 025; R. V. Harlander, T. Neumann, K. J. Ozeren, and M. Wiesemann, *J. High Energy Phys.* **08** (2012) 139; M. Grazzini and H. Sargsyan, *J. High Energy Phys.* **09** (2013) 129; A. Banfi, P. F. Monni, and G. Zanderighi, *J. High Energy Phys.* **01** (2014) 097.
- [15] M. Spira, *Fortschr. Phys.* **46**, 203 (1998).
- [16] T. Plehn, M. Spira, and P. M. Zerwas, *Nucl. Phys.* **B479**, 46 (1996); **B531**, 655 (1998); U. Baur, T. Plehn, and D. L. Rainwater, *Phys. Rev. Lett.* **89**, 151801 (2002); M. J. Dolan, C. Englert, and M. Spannowsky, *J. High Energy Phys.* **10** (2012) 112; J. Grigo, J. Hoff, K. Melnikov, and M. Steinhauser, *Nucl. Phys.* **B875**, 1 (2013); *Phys. Rev. D* **89**, 013012 (2014).
- [17] D. S. M. Alves, M. R. Buckley, P. J. Fox, J. D. Lykken, and C.-T. Yu, *Phys. Rev. D* **87**, 035016 (2013); S. Bornhauser, M. Drees, S. Grab, and J. S. Kim, *Phys. Rev. D* **83**, 035008 (2011); N. Desai and B. Mukhopadhyaya, *J. High Energy Phys.* **05** (2012) 057; Z. Han, A. Katz, D. Krohn, and M. Reece, *J. High Energy Phys.* **08** (2012) 083; G. Belanger, R. M. Godbole, L. Hartgring, and I. Niessen, *J. High Energy Phys.* **05** (2013) 167; X.-Q. Li, Z.-G. Si, K. Wang, L. Wang, L. Zhang, and G. Zhu, *Phys. Rev. D* **89**, 077703 (2014).
- [18] R. K. Ellis, I. Hinchliffe, M. Soldate, and J. J. van der Bij, *Nucl. Phys.* **B297**, 221 (1988).
- [19] U. Baur and E. W. N. Glover, *Nucl. Phys.* **B339**, 38 (1990).
- [20] M. Schlaffer, M. Spannowsky, M. Takeuchi, A. Weiler, and C. Wymant, [arXiv:1405.4295](https://arxiv.org/abs/1405.4295).
- [21] A. Banfi, A. Martin, and V. Sanz, [arXiv:1308.4771](https://arxiv.org/abs/1308.4771).
- [22] R. V. Harlander and T. Neumann, *Phys. Rev. D* **88**, 074015 (2013).
- [23] A. Azatov and A. Paul, *J. High Energy Phys.* **01** (2014) 014.
- [24] C. Grojean, E. Salvioni, M. Schlaffer, and A. Weiler, *J. High Energy Phys.* **05** (2014) 022.
- [25] C. Englert, M. McCullough, and M. Spannowsky, *Phys. Rev. D* **89**, 013013 (2014).
- [26] T. Plehn, D. L. Rainwater, and D. Zeppenfeld, *Phys. Rev. Lett.* **88**, 051801 (2002); C. Ruwiedel, N. Wermes, and M. Schumacher, *Eur. Phys. J. C* **51**, 385 (2007); G. Klamke and D. Zeppenfeld, *J. High Energy Phys.* **04** (2007) 052; K. Hagiwara, Q. Li, and K. Mawatari, *J. High Energy Phys.* **07** (2009) 101; C. Englert, D. Goncalves-Netto, K. Mawatari, and T. Plehn, *J. High Energy Phys.* **01** (2013) 148; C. Englert, D. Goncalves, G. Nail, and M. Spannowsky, *Phys. Rev. D* **88**, 013016 (2013); K. Hagiwara

- and S. Mukhopadhyay, *J. High Energy Phys.* **05** (2013) 019; M.R. Buckley, T. Plehn, and M.J. Ramsey-Musolf, [arXiv:1403.2726](https://arxiv.org/abs/1403.2726).
- [27] V. Del Duca, W. Kilgore, C. Oleari, C. Schmidt, and D. Zeppenfeld, *Phys. Rev. Lett.* **87**, 122001 (2001); V. Del Duca, W. Kilgore, C. Oleari, C. Schmidt, and D. Zeppenfeld, *Nucl. Phys.* **B616**, 367 (2001).
- [28] E. Boos and T. Plehn, *Phys. Rev. D* **69**, 094005 (2004).
- [29] J. M. Campbell, R. K. Ellis, R. Frederix, P. Nason, C. Oleari, and C. Williams, *J. High Energy Phys.* **07** (2012) 092; J. M. Campbell, R. K. Ellis, and C. Williams, MCFM web page <http://mcfm.fnal.gov>.
- [30] F. Campanario, M. Kubocz, and D. Zeppenfeld, *Phys. Rev. D* **84**, 095025 (2011); J. Baglio *et al.*, [arXiv:1404.3940](https://arxiv.org/abs/1404.3940); K. Arnold *et al.*, *Comput. Phys. Commun.* **180**, 1661 (2009).
- [31] T. Sjostrand, S. Mrenna, and P.Z. Skands, *J. High Energy Phys.* **05** (2006) 026.
- [32] J. M. Campbell, R. K. Ellis, and G. Zanderighi, *J. High Energy Phys.* **10** (2006) 028; J. M. Campbell, R. K. Ellis, and C. Williams, *Phys. Rev. D* **81**, 074023 (2010); H. van Deurzen, N. Greiner, G. Luisoni, P. Mastrolia, E. Mirabella, G. Ossola, T. Peraro, J. F. von Soden-Fraunhofen, and F. Tramontano, *Phys. Lett. B* **721**, 74 (2013).
- [33] S. Frixione, P. Nason, and C. Oleari, *J. High Energy Phys.* **11** (2007) 070; T. Melia, P. Nason, R. Rontsch, and G. Zanderighi, *J. High Energy Phys.* **11** (2011) 078.
- [34] T. Gleisberg, S. Hoeche, F. Krauss, M. Schonherr, S. Schumann, F. Siegert, and J. Winter, *J. High Energy Phys.* **02** (2009) 007; C. F. Berger, Z. Bern, L. J. Dixon, F. Febres Cordero, D. Forde, H. Ita, D. A. Kosower, and D. Maitre, *Phys. Rev. D* **78**, 036003 (2008); T. Gleisberg and S. Hoeche, *J. High Energy Phys.* **12** (2008) 039; S. Hoeche, F. Krauss, M. Schonherr, and F. Siegert, *J. High Energy Phys.* **09** (2012) 049; **08** (2011) 123; S. Hoeche, F. Krauss, M. Schonherr, and F. Siegert, *J. High Energy Phys.* **04** (2013) 027; S. Hoeche, F. Krauss, and M. Schonherr, [arXiv:1401.7971](https://arxiv.org/abs/1401.7971).
- [35] M. Cacciari, G. P. Salam, and G. Soyez, *J. High Energy Phys.* **04** (2008) 063; M. Cacciari, G. P. Salam, and G. Soyez, *Eur. Phys. J. C* **72**, 1896 (2012).
- [36] C. Englert, M. Spannowsky, and M. Takeuchi, *J. High Energy Phys.* **06** (2012) 108; C. Bernaciak, M. S. A. Buschmann, A. Butter, and T. Plehn, *Phys. Rev. D* **87**, 073014 (2013).